Materials Science and Engineering A 510–511 (2009) 175–179

Contents lists available at ScienceDirect

Materials Science and Engineering A

journal homepage: www.elsevier.com/locate/msea

Life-time prediction for advanced low alloy steel P23

Philipp von Hartrott[a,*], Stefan Holmström[b], Stefano Caminada[c], Sylvain Pillot[d]

[a] Fraunhofer Institut für Werkstoffmechanik IWM, Wöhlerstr. 11, 79108 Freiburg, Germany
[b] VTT, P.O. Box 1000 FI-02044 VTT, Finland
[c] TenarisDalmine, Piazza Caduti 6 Luglio 1944, 1 – 24044 Dalmine, Italy
[d] Centre de Recherche des Matériaux du Creusot - Industeel - ArcelorMittal group, 56, rue Clémenceau - BP19 - 71201 Le Creusot Cedex, France

ARTICLE INFO

Article history:
Received 9 January 2008
Received in revised form 19 February 2008
Accepted 30 April 2008

Keywords:
T23
P23
Creep strain
Creep rupture
TMF
LCF
Modeling

ABSTRACT

Lifetime models for both creep and thermo-mechanical fatigue are presented for P23 steel. The models are the result of the joint European RFCS project ALoAS. The creep model, developed for robust creep strain modeling, here adjusted to describe the strain response of the ALoAS data, i.e. P23 pipe material fabricated by TenarisDalmine and plate material heat fabricated by Industeel. The creep modeling range covers 550–660 °C in temperature and 80–180 MPa in stress. The thermo-mechanical fatigue model is adjusted to the acquired data on thick walled P23 pipe material fabricated by TenarisDalmine. The load range covers 20–625 °C and up to 16,000 cycles to failure. A good description of the data has been achieved for both creep and fatigue models.

1. Introduction

One of the main objectives in the ALoAS project is to assess the mechanical behaviour of the new heat resistant low alloy steels T/P23 and T24. Special effort has been put into developing weld materials and welding procedures for reliable high temperature welds. By definition this leads to extensive testing of both the parent materials and the produced weldments. The assessments of the ALoAS creep, low cycle fatigue (LCF) and thermo-mechanical fatigue (TMF) tests are here presented for insight in the potential life prediction of these materials for use at high temperatures. The mechanical testing together with modeling and simulation aspects aims to reliably assess the potential of this material for large complex components under realistic loading conditions in the form of creep and TMF. It is shown that the required tools and data for both high-temperature creep and TMF models are in place for robust life predictions.

2. Materials

The base materials adopted for the experimental activity were supplied by Tenaris and Industeel. In particular Tenaris supplied grade 23 seamless tubes and pipes according to, respectively, ASTM A213 and A335 standards. From the six heats produced for the project, all six were creep tested and one was selected for thorough TMF characterisation and component testing (OD × WT 88.9 × 17 mm). The component testing pipes were produced in the TenarisDalmine continuous mill by piercing and hot rolling hot rolled billets from heat 109194 (Table 1). After hot rolling the pipes were quenched and tempered to obtain a full tempered bainitic microstructure, as shown in Fig. 1. The mechanical properties of the pipes fully comply with ASTM A335 standard, as shown in Table 2.

3. Creep

Six heats of T/P23 have been creep tested, five pipe (and tube) products and one plate product form. To date the maximum durations in creep testing (for the parent material) is approaching 20,000 h. The maximum rupture times are expected to reach at least 30,000 h, running well beyond the ALoAS project. The creep assessments presented in this paper are based on creep data available in June 2007, and is therefore to be considered an intermediate result.

3.1. Creep rupture modeling

The presented intermediate creep rupture master curve for parent P23 has been assessed on a multi-heat data set consisting of the ALoAS data together with selected public domain data and standard

* Corresponding author. Tel.: +49 761 5142 273; fax: +49 761 5142 404.
E-mail address: philipp.von.hartrott@iwm.fraunhofer.de (P. von Hartrott).

0921-5093/$ – see front matter © 2008 Elsevier B.V. All rights reserved.
doi:10.1016/j.msea.2008.04.117

Table 1
Chemical composition in mass % of the tubes OD × WT 88.9 × 17 mm.

Material	C	Mn	Si	S	P	Cr	Mo	Ni	B (ppm)	N	Ti	V	Al	Cu	Nb	W
ASTM A335 P23	0.04	0.10	–	–	–	1.90	0.05	–	5	–	–	0.20	–	–	0.02	1.45
	0.10	0.60	0.50	0.010	0.030	2.60	0.30	–	60	0.030	–	0.30	0.030	–	0.08	1.75
Heat 109194	0.067	0.46	0.26	0.005	0.009	2.1	0.11	0.13	24	0.008	0.027	0.21	0.019	0.14	0.045	1.58

Table 2
Mechanical properties of the base material.

Pipe size OD × WT	Heat	YS		UTS		Elongation	
		Actual	ASTM	Actual	ASTM	Actual	ASTM
88.9 × 17 mm	109194	517 MPa	>400 MPa	620 MPa	>510 MPa	35%	>20%

values [1,2]. The general trends of P23, HCM2S (Japanese T/P23) and P22 (EN10216-2 values) rupture models are shown in Fig. 2. The master equation of P23 was acquired by data fitting with the DESA software tool (Technische Universität Darmstadt) [3]. The selected (mathematically best fitting) model is the multi-linear form of the minimum commitment model. The intermediate model is considered sufficient for extrapolations to at least 30,000 h and for finite element analysis modeling purposes. At this stage the model has not been post-assessment tested and all long-term data has not been incorporated in the assessment. A fully ECCC compliant [4] rupture model with extended extrapolation capabilities is expected at the end of the ALoAS project.

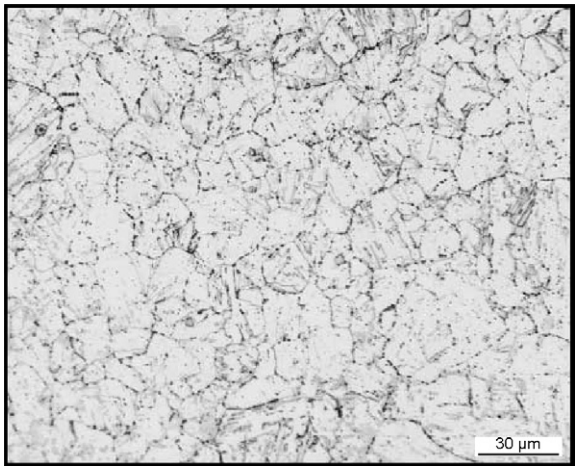

Fig. 1. tempered bainitic microstructure of tubes ODxWT 88.9 × 17 mm (mid-thickness).

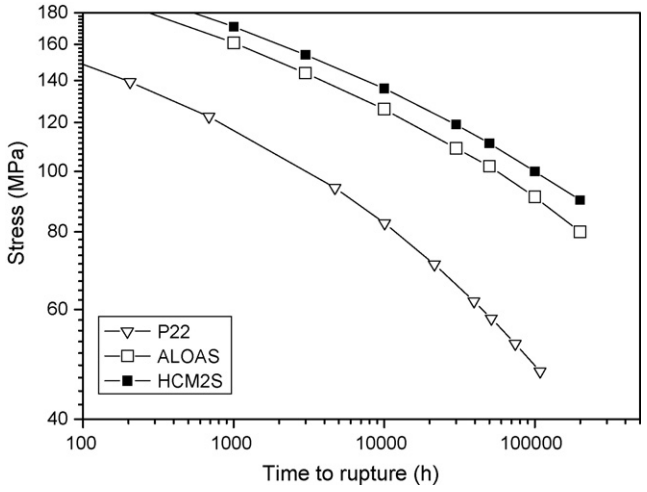

Fig. 2. Intermediate creep rupture modeling results at 575 °C, for ALoAS P23 (open squares) in comparison to HCM2S (black squares, fit from data in Ref. [1]) and P22 (triangles, fit from ECCC short-term data and EN-10216 standard values). Note that the P23 long-term creep strength has been extrapolated beyond recommended limits in time.

The intermediate minimum commitment master curve for rupture is defined in the following equation and the model constants β_1–β_5 are presented in Table 3:

ALoAS P23 time to rupture (t_r) as a function of temperature (K) and stress (σ_0):

$$\log(t_r) = \frac{\beta_0 + \beta_1 \log[\sigma_0] + \beta_2 \sigma_0 + \beta_3 \sigma_0^2 + \beta_4 T + \beta_5}{T} \quad (1)$$

3.2. Creep strain modeling

Creep strain modeling for P23 has also been performed. The modeling was done using the logistic creep strain prediction method (LCSP [5]) partly developed within the ALoAS project. In its uniaxial form it can predict the full creep curves using the time to creep rupture as base. It predicts primary, secondary and tertiary creep as a function of time to rupture, temperature and stress. The minimum strain rates, primary strain and linear strain are predicted for P23 (by LCSP) for rupture times 10,000, 30,000 and 100,000 h (see Table 5). Also the parameters for the simple Norton law were extracted for direct use in the finite element analysis program ABAQUS creep module. The definitions of predicted primary, linear and minimum strain rate are given in Fig. 3. The LCSP (Eq. (2)) defining the whole creep curve and the Norton law (Eq. (3)) for minimum creep strain rate are defined as follows:

$$\log\ \varepsilon_t = \left(\frac{\log t_r + C}{\log t_\varepsilon + C} - 1\right)^{1/p} x_0 \quad (2)$$

$$\dot{\varepsilon}_{\min} = A\sigma^n \quad (3)$$

Table 3
Creep rupture P23 multi-heat master equation constants.

β_0	24.6826
β_1	2.0101
β_2	−0.04125
β_3	0.00002223
β_4	−0.02622
β_5	1850.03

Table 4
Creep strain master equation constants for creep strain (parent P23). *Note*: Stress in MPa.

$x_0(\sigma,T)$	$4.21 + 0.69601 \times \log\sigma - 7860/(T+273)$
$p(\sigma,T)$	$14.3 - 2.271 \times \log\sigma + 4829/(T+273)$
C	3.5

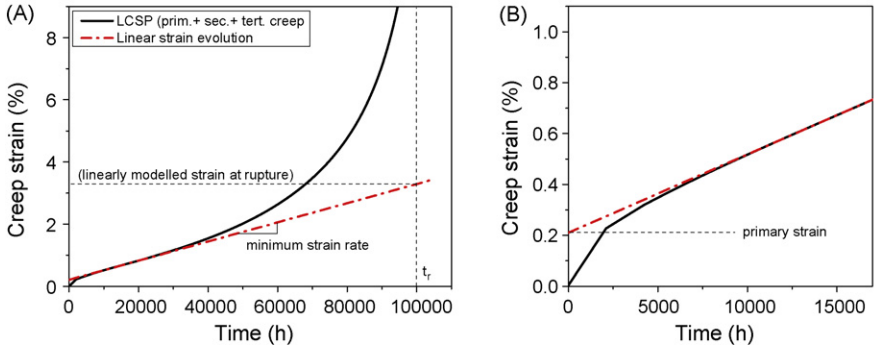

Fig. 3. Creep strain prediction (LCSP and Norton type) for P23 at 575 °C/91 MPa (predicted rupture at 100,000 h); A: full creep curve, B: close-up on primary creep stage.

Table 5
Norton law fitting parameters, primary strain, linear strain at rupture and minimum strain rates (1/h) for P23 steel, acquired from LCSP master equation at 550–625 °C (see Fig. 3). Note that the 100,000 h rupture in parenthesis is beyond recommended extrapolation range for the available data set.

Time t_r (h)	Temp (°C)	Stress (MPa)	Norton law parameters		Prim. strain (%)	Lin. strain at t_r (%)	Min. strain rate (h^{-1})
			n	log$A$			
10,000	550	150	10.78	−28.93	0.16	3.86	3.386×10^{-6}
30,000	550	135	9.91	−27.05	0.17	3.63	1.174×10^{-6}
(100,000)	550	116	8.72	−24.53	0.17	3.28	2.997×10^{-7}
10,000	575	126	9.27	−24.94	0.22	3.71	3.433×10^{-6}
30,000	575	110	8.24	−22.78	0.22	3.41	1.093×10^{-6}
(100,000)	575	91	6.86	−19.98	0.21	3.00	2.582×10^{-7}
10,000	600	101	7.56	−20.63	0.29	3.56	3.258×10^{-6}
30,000	600	84	6.35	−18.24	0.27	3.14	9.67×10^{-7}
(100,000)	600	63	4.76	−15.23	0.24	2.52	2.194×10^{-7}
10,000	625	74	5.55	−15.93	0.34	3.26	2.763×10^{-6}
(30,000)	625	56	4.15	−13.36	0.30	2.66	8.001×10^{-7}
(100,000)	625	30	2.48	−10.52	0.20	1.63	1.394×10^{-7}

where ε_t is the predicted strain at time t_ε, t_r is the rupture time in hours, $\dot{\varepsilon}$ the minimum strain rate, and p, x_0, A and n are constants (n = Norton creep exponent). The creep strain master equation constants for P23 are given in Table 4. The LCSP has also been utilised directly with the VTT "in house routines" developed for simulating complex component creep response [6].

The creep rupture model together with the creep strain model give a sound base for life management of the material within the creep regime.

4. Fatigue

4.1. Experiments

The round LCF specimen with a working section of 7 mm diameter and 17 mm length where taken axially from a pipe of the described heat 109194. The LCF and TMF experiments were performed on an Instron servo-hydraulic testing machine using an inductive heating system. Strains were measured using a MAYTEC high temperature extensometer with a reference length of 10 mm. Strain controlled complex LCF experiments where performed at 20, 400, 450, 550, 575, 600 and 625 °C. The complex LCF experiments consist of two parts: the first complex part covers strain rates from 10^{-5} s^{-1} to 10^{-3} s^{-1}, hold times of 30 min in tension and compression and different strain amplitudes. In the second part a triangular strain shape with a strain rate of 10^{-3} s^{-1} and strain amplitudes between 0.25% and 0.5% depending on the temperature are applied to the specimen until failure. Failure is defined as a 5% drop of the stress envelope. A TMF experiment was performed in the temperature range 325–625 °C with a cycle time of 250 s. The gauge length was held constant during the thermal cycle so that all thermal strain was constrained.

At all temperatures the material displays cyclic softening, with a ratio of the initial maximum stress to the maximum stress at half of the cycles to failure ($N_f/2$) ranging from 1.09 at 20 °C to 1.43 at 625 °C.

The cycles to failure range from 1392 at 625 °C and a strain amplitude of 0.3% to 16018 at 400 °C and a strain amplitude of 0.25%. Fig. 4 shows the results of the LCF experiments. The TMF experiment reached 1709 cycles to failure.

4.2. TMF modeling

The TMF model is based on the description of the viscoplastic deformation at the crack tip, namely the crack tip opening displacement during a load cycle. Hence, the description of the

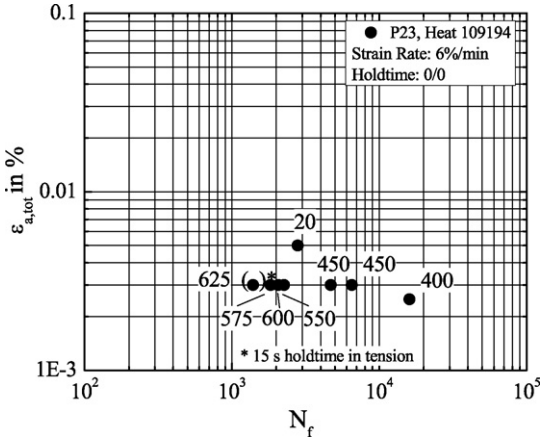

Fig. 4. Experimental cycles to failure for different temperatures and strain amplitudes.

Table 6
Parameters of the viscoplastic deformation model.

	20 °C	400 °C	450 °C	550 °C	575 °C	600 °C	625 °C
E	2.07e+05	1.98e+05	1.85e+05	1.73e+05	1.69e+05	1.66e+05	1.62e+05
α_{dif}^{th}	1.38e+05	1.71e+05	1.75e+05	1.83e+05	1.85e+05	1.88e+05	1.90e+05
K	1.29e+02	2.85e+02	3.32e+02	4.63e+02	5.09e+02	5.58e+02	7.25e+02
n	3.87e+00	2.88e+00	2.65e+00	2.49e+00	2.47e+00	2.46e+00	2.46e+00
σ_Y	0.00e+00	0.00e+00	0.00e+00	0.00e+00	0.00e+00	0.00e+00	0.00e+00
Q_∞	0.00e+00	0.00e+00	0.00e+00	0.00e+00	0.00e+00	0.00e+00	0.00e+00
b	0.00e+00	0.00e+00	0.00e+00	0.00e+00	0.00e+00	0.00e+00	0.00e+00
C^1/γ^1	2.16e+02	2.04e+02	1.97e+02	1.73e+02	1.20e+02	8.22e+01	7.39e+01
γ^1	1.62e+02	5.03e+02	8.50e+02	9.67e+02	1.10e+03	1.21e+03	1.46e+03
R^1	4.71e+08	1.36e+04	1.80e+04	3.27e+04	8.27e+04	9.14e+04	3.76e+03
Φ_∞^1	6.50e+01	6.80e+01	7.60e+01	8.40e+01	8.80e+01	8.90e+01	9.00e+01
ω^1	3.00e+00	1.00e+01	1.20e+01	1.40e+01	1.50e+01	2.10e+01	2.30e+01
C^2/γ^2	4.12e+02	3.29e+02	2.35e+02	1.86e+02	1.85e+02	1.85e+02	1.84e+02
γ^2	3.50e+03	5.86e+03	6.98e+03	8.34e+03	9.86e+03	7.37e+03	6.80e+03
R^2	0.00e+00	0.00e+00	0.00e+00	0.00e+00	0.00e+00	0.00e+00	0.00e+00
Φ_∞^2	1.20e+00	1.23e+00	1.46e+00	2.17e+00	2.20e+00	1.85e+00	2.24e+00
ω^2	5.23e+01	7.88e+01	9.06e+01	4.55e+01	5.31e+01	5.60e+01	5.93e+01

TMF behavior requires a description of the viscoplastic deformation behavior of the material and a description of the damage evolution.

4.2.1. Deformation model

All essential phenomena of cyclic plasticity and high-temperature deformation of metals can be described by time- and temperature-dependent material models after Chaboche [7]. The constitutive equations of the model are given below for the case of uniaxial deformation.

Total strain rate:

$$\dot{\varepsilon} = \frac{\dot{\sigma}}{E} + \dot{\varepsilon}^{vp} + \dot{\varepsilon}^{th} \tag{4}$$

Viscoplastic strain rate:

$$\dot{\varepsilon}^{vp} = \dot{p} sgn(\sigma - \alpha) \text{ where } \dot{p} = \left\langle \frac{|\sigma - \alpha| - R}{K} \right\rangle^n \tag{5}$$

Thermal strain rate:

$$\dot{\varepsilon}^{th} = \alpha_{dif}^{th} \dot{\theta} \tag{6}$$

Isotropic hardening:

$$R = \sigma_Y + Q_\infty(1 - \exp[-bp]) \tag{7}$$

Kinematic hardening:

$$\alpha = \sum_{a=1}^{2} \alpha^a \text{ where } \dot{\alpha}^a = C^a \dot{\varepsilon}^{vp} - \gamma^a \Phi^a \alpha^a \dot{p} - R^a \alpha^a + \frac{1}{C^a} \frac{\partial C^a}{\partial \theta} \alpha^a \dot{\theta} \tag{8}$$

Cyclic hardening/softening functions:

$$\Phi^1 = \Phi_\infty^1 + (1 - \Phi_\infty^1) \exp(-\omega^1 |\varepsilon^{vp}|) \tag{9}$$

$$\Phi^2 = \Phi_\infty^2 + (1 - \Phi_\infty^2) \exp(-\omega^2 p) \tag{10}$$

E is the Young's modulus (MPa); α_{dif}^{th} is the differential coefficient of thermal expansion (1/°C); K is the reference stress of viscosity (MPa); n is the strain rate exponent (−); σ_Y is the yield stress (MPa); Q_∞ is the threshold of isotropic hardening (MPa); b is the transition constant (−); C^a/γ^a is the threshold of kinematic hardening (MPa); γ^a is the transition constant of dynamic recovery (−); R^a is the transition constant of static recovery (s^{-1}); Φ_∞^a is the saturation value of cyclic hardening/softening (−); ω^a is the transition constant of cyclic hardening/softening (−).

All the above parameters are temperature dependent. For non-isothermal loading the model parameters are obtained by a linear interpolation in temperature.

The model for cyclic plasticity was adjusted to the experimental results of the complex LCF experiments. The resulting model is capable of predicting the viscoplastic behavior of the material under non-isothermal loading conditions. Fig. 5 shows the application of the model to thermo-cyclic loading. The resulting model parameters are given in Table 6. The finite element implementation [8] is capable of handling large size problems in acceptable computing time.

4.2.2. Damage model

For many steels, the lifetime under cyclic or thermo-cyclic loading is controlled by the formation and growth of microcracks. On the basis of elastic–plastic fracture mechanics, Heitmann [9] developed a damage parameter Z_D for room temperature applications. For high temperature applications Riedel [10] proposed the D_{CF}-parameter (CF for creep–fatigue). The damage parameter D_{TMF} is an extension of D_{CF} for non-isothermal cycles of arbitrary shape [11]. It has been studied on different materials [12]. Its functional form is

$$D_{TMF} = \left(1.45 \frac{\Delta\sigma_{I,eff}^2}{\sigma_{cy} E} + \frac{2.4}{\sqrt{1+3N}} \frac{\Delta\sigma_I^2}{\sigma_{cy} \Delta\sigma_e} \Delta\varepsilon_e^{in} \right) F. \tag{11}$$

σ_{cy} is the cyclic yield stress, N the Ramberg-Osgood hardening exponent of the cyclic stress–strain curve and E is Young's modulus. These parameters can be determined from LCF-hysteresis loops.

$\Delta\sigma$ and $\Delta\varepsilon^{in}$ are twice the stress and plastic strain amplitudes, respectively.

Further, the von Mises equivalent stress amplitude, the maximum principal stress amplitude and the equivalent plastic strain

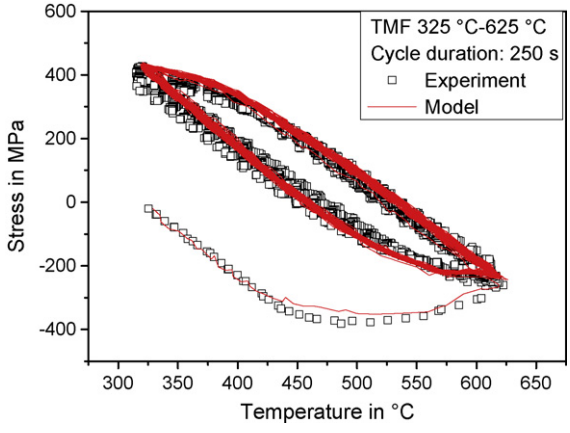

Fig. 5. Stress–temperature hysteresis of the TMF experiment (first 30 cycles).

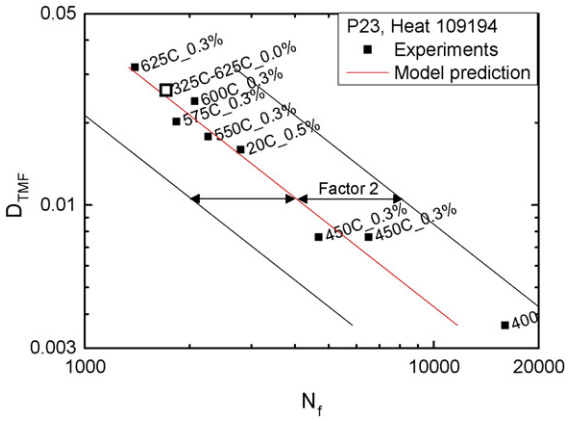

Fig. 6. Experimental and predicted cycles to failure.

amplitude are given by

$$\Delta\sigma_e = \sqrt{\frac{2}{3}(\boldsymbol{\sigma}' - \boldsymbol{\sigma}'^0) : (\boldsymbol{\sigma}' - \boldsymbol{\sigma}'^0)} \tag{12}$$

$$\Delta\sigma_I = |\sigma_H - \sigma_H^0| \tag{13}$$

$$\Delta\varepsilon_e^{in} = \sqrt{\frac{2}{3}(\varepsilon^{in\prime} - \varepsilon^{in\prime 0}) : (\varepsilon^{in\prime} - \varepsilon^{in\prime 0})}. \tag{14}$$

The superscript 0 indicates the start point of the cycle. σ_H is the principal stress having the greatest amount, thus $\sigma_H = \max(|\sigma_I|, |\sigma_{III}|)$.

The effective amplitude takes the effect of crack closure into account:

$$\Delta\sigma_{I,eff} = \frac{3.72}{(3-R)^{1.74}}\Delta\sigma_I \tag{15}$$

R is the ratio of minimum to maximum stress in a load cycle. The factor F in the expression for D_{TMF} takes the temperature-time history into account, especially the effect of hold times.

The results of the LCF and TMF experiments can be uniformly described using the damage parameter D_{TMF}. All experiments can be predicted within a scatter band significantly smaller than factor two. Fig. 6 shows the predicted and measured cycles to failure for the LCF and TMF experiments.

5. Summary

Results of an intermediate creep data assessment and final assessment results of low cycle and TMF on T/P23 have been presented. The P23 creep rupture properties have been compared to HCM2s and the reference material P22. A robust creep strain model (LCSP) has been presented and adjusted to the acquired data. A good description of the experimental data has been achieved. A Chaboche-type model for cyclic plasticity has been presented and adjusted to the acquired P23 data. A damage model based on the D_{TMF} damage parameter for TMF has been presented and applied to the experimental data. Both, the thermo-mechanical deformation and the damage model describe the experimental findings well.

6. Conclusion

An extensive set of material properties for life assessment of P23 (ALoAS materials) in high-temperature applications like conventional power plants have been determined. The acquired data on creep rupture, creep strain, low cycle- and thermo-mechanical fatigue support the introduction of the tested material into industrial application.

The creep modeling of the material resulted in industrially applicable models for creep rupture, creep strain, including the full creep curve at specified stress and temperature. As a by-product the Norton parameters for steady state modeling finite element analysis have been acquired. The TMF model has been derived for data from one heat. Its implementation is available for large sized finite element models.

A comprehensive data and modeling tool set for lifetime prediction of the T-P23 steel is now available.

Acknowledgements

This work has been made with the financial support of the European Community Research Fund for Steel and Coal, ALoAS, Project Number PR02033, September 2003–February 2008.

References

[1] N. Komai, T. Imazato, Effect of tempering times on creep strength in ASME Gr. 23 (2.25 Cr-1.6 W steel), Materials for Advanced Power Engineering 2006, in: J. Lecomte-Beckers, et al. (Eds.), Proceedings of the 8th Liège Conference, II, 2006, pp. 997–1009.
[2] EN 10216-2, 2002+A2: 2007. Technical Delivery Conditions. Part 2. Non-alloy and Alloy Steel Tubes with Specified Elevated Temperature Properties, CEN, Brussels, 2007.
[3] J. Granacher, M. Monsees, P. Hillenbrand, C. Berger, in: A.S. Jovanovic (Ed.), SMIRT Post Conference Seminar, No. 13, August 25–27, 1997, Proc., MPA Stuttgart, S. 179–195.
[4] ECCC recommendations, Creep data validation and assessment procedures, S.R. Holdsworth et al. (Eds.) ERA Technology publ., 2001 (a) Vol 1: Overview, (b) Vol 2. Terms and Terminology, (c) Vol 3. Data Acceptability Criteria, Data Generation, (d) Vol 4. Data Excange and Collation, (e) Vol 5. Data assessment.
[5] S. Holmström, P. Auerkari, Robust prediction of full creep curves from minimal data and time to rupture model, Energy Materials. Institute of Materials, Vol. 1., 2006, No. 4, pp. 249–255.
[6] S. Holmström, A. Laukkanen, K. Calonius, Weldment matching for creep life of P22 and P91 girth welds, International Conference on Integrity of High Temperature Welds, 24–26 April 2007, London, UK. Conf. Proc. IOM Communications publication, ISBN-1-86125-166-1. pp. 245–255.
[7] J.L. Chaboche, Int. J. Plast. 5 (1989) 247–302.
[8] T. Seifert, I. Schmidt, Line-search methods in general return mapping algorithms with application to porous plasticity, Int. J. Numer. Meth. Eng. 73 (2007) 1468–1495.
[9] H. Heitmann Betriebsfestigkeit von Stahl: Vorhersage der technischen Anrisslebensdauer unter Berücksichtigung des Verhaltens von Mikrorissen, Diss. RWTH Aachen, 1983.
[10] H. Riedel, Fracture at High Temperatures, Springer Verlag, Berlin, Heidelberg, New York, 1987.
[11] W. Schmitt, R. Mohrmann, H. Riedel, A. Dietsche, in: A.F. Blom (Ed.), Fischersworring-Bunk, A. "Modelling of the Fatigue Life of Automobile Exhaust Components", Fatigue 2002, Engineering Materials Advisory Services Ltd., Cradley Heath, U.K., 2002, pp. 781–788.
[12] C. Schweizer, T. Seifert, M. Schlesinger, H. Riedel, Korrelation zwischen zyklischer Risspitzenöffnung und Lebensdauer, Conference Proceedings of 39. Tagung des DVM-Arbeitskreis Bruchvorgänge, DVM Report 239, Dresden, 2007, pp. 237–246.